Detailed in Situ XRD and Calorimetric Study of the Formation of Silicate/Mixed Surfactant Mesophases under Alkaline Conditions. Influence of Surfactant Chain Length and Synthesis Temperature

Isabelle Beurroies,[†,‡] Patrik Ågren,[‡] Gunter Büchel,[†] Jarl B. Rosenholm,[‡] Heinz Amenitsch,[§] Renaud Denoyel,[†] and Mika Linden*[,‡]

MADIREL (CNRS-Université de Provence), Centre de St Jérôme, 13397 Marseille Cedex 20, France, Department of Physical Chemistry, Åbo Akademi University, Porthansgatan 3-5, FIN-20500 Turku, Finland, and Institute of Biophysics and X-ray Structure Research, Austrian Academy of Sciences, Schmiedlstrasse 6, A-8042 Graz, Austria

Received: July 8, 2005; In Final Form: June 4, 2006

The formation of mesoscopically ordered silica/surfactant composites under alkaline synthesis conditions has been studied by time-resolved in situ small-angle X-ray diffraction with synchrotron radiation. Alkyltrimethylammoniumbromide surfactants, C_nTAB, of different chain lengths ($n = 14$, 16, and 18) as well as mixtures thereof were used as structure directing agents and the measurements were carried out at two different temperatures. A linear relationship between the mean surfactant chain length and the *d* spacing of the hexagonal phase was observed, suggesting an ideal mixing of the surfactants in the supramolecular surfactant aggregates. It is shown that the formation of the hexagonal phase is kinetically controlled mainly by the rate of silicate condensation, while the effect of changes in the surfactant chain length on the kinetics is small under the studied conditions. Two concominant, albeit partly interlinked, processes, suggested being intra- and intermicellar condensation, followed by aggregate−aggregate condensation, govern the nucleation and growth of the hexagonal phase. The two-step mechanism is confirmed by a microcalorimetric study where the heat evolved during the hydrolysis−condensation reactions is followed as a function of time.

Introduction

The synthesis of mesoscopically ordered organic−inorganic composite materials, which can be made mesoporous upon removal of the organic structure-directing agent, is a growing field of research. Supramolecular surfactant aggregates serve as structure directors in the synthesis of such materials,[1,2] typically metal oxides, and most of the different liquid crystalline phases observed for surfactants have been observed for the composite materials as well. The formation of the mesostructure in dilute systems is a cooperative process, where the early stages of the formation are governed by interactions between the surfactant molecules and partially condensed oxo-hydroxo species.[3−5] The most studied member of this group of silicate materials is MCM-41, which has a 2D hexagonal symmetry.[1,2] MCM-41 is synthesized under alkaline conditions typically with alkyltrimethylammonium salts as the surfactant. It has been shown that the mesopore diameter of the final material is dependent on the chain length surfactant used as the structure-directing agent in the synthesis.[1,2] Further fine-tuning of the pore diameter is possible if a mixture of cationic surfactants with different headgroups[6] or of different chain lengths[7,8] is used as structure directing agents. Various in situ techniques have been applied to investigate the kinetics of silicate−surfactant mesophase formation and to study the reaction mechanisms, as recently reviewed by Patarin et al.[9] and Edler.[10] It was long assumed that intact surfactant micelles serve as the building blocks around which the silicate condenses. However, recent fluorescence quenching studies[5] suggest that the surfactant micelles only serve as a pool for surfactant and that surfactant monomers are adsorbed to partially condensed oppositely charged silicate units. These surfactant−silicate, i.e., inorganic polyelectrolyte−surfactant, complexes cooperatively assemble to form the silicatropic mesophase. Furthermore, time-resolved in situ small-angle X-ray scattering and diffraction studies have been extensively used to study the kinetics of the self-assembly process of mesostructured silica,[11−21] zirconia,[22,23] titania,[22] or aluminum phosphates.[24] The use of synchrotron radiation enables detailed studies to be carried out due to the short data acquisition times needed. Most, if not all, previous in situ XRD studies of the MCM-41 formation process have been carried out on systems where C_{16}TAB has been used as the main structure-directing agent. However, the use of surfactants of different chain length under otherwise similar experimental conditions could shed some light on the influence of the micellar geometry on the formation kinetics of the mesophase, since the formation of rodlike micelles is favored by an increase in the surfactant chain length due to the increase in the attractive van der Waals forces between the surfactants in the micelle. We have therefore performed an in situ synchrotron XRD investigation of the formation of MCM-41 studied as a function of the mean chain length of the alkyltrimethylammoniumbromide surfactant used as the structure-directing agent, at two different synthesis temperatures. A thorough data analysis makes it possible to study the reaction in more detail than what has been reported previously by us and others, where the XRD data mostly have been analyzed in a qualitative fashion. The synthesis

* To whom correspondence should be addressed. E-mail: mlinden@abo.fi.
† MADIREL.
‡ Åbo Akademi University.
§ Austrian Academy of Sciences.

10.1021/jp053746y CCC: $33.50
Published on Web 07/22/2006

composition chosen is ideally suited for in situ synchrotron studies, since the silicate hydrolysis and condensation reactions are relatively fast in the presence of the surfactant micelles at the synthesis pH of about 10.7, and mesophase formation occurs within a couple of minutes under ambient conditions.[12,13] Microcalorimetry was also used to follow the heat evolved by the various reactions that occur during the synthesis.

Experimental Section

The measurements were conducted at the Austrian SAXS beamline[25] at the electron storage ring ELETTRA, Trieste, Italy, utilizing a linear position-sensitive Gabriel detector. The SAXS camera was set to a length of 1.5 m and to a photon energy of 8 keV. The reactions were carried out in a batch reactor described elsewhere[16] at either 30 or 40 °C by the following procedure: binary aqueous solutions of alkyltrimethylammoniumbromide (C_nTAB, $n = 14$, 16, or 18; Sigma-Aldrich) were prepared to which ammonia (25% NH_3) was added. Data acquisition was triggered by the addition of tetraethyl orthosilicate (TEOS, Sigma Aldrich; i.e., $t = 0$ s) to the surfactant solutions; 1024 frames were recorded in total with a time resolution of 10 s in the beginning, 0.5 s during the formation of the hexagonal phase, and 5 s at later stages. The diffraction patterns have been normalized for primary intensity fluctuations and the background scattering from a water filled capillary has been subtracted. The molar composition of the reaction mixtures was H_2O/NH_3/CTAB/TEOS = 165/3.7/0.14/1 for the C_{14}TAB−C_{16}TAB series and H_2O/NH_3/CTAB/TEOS = 165/3.7/0.11/1 for the C_{16}TAB−C_{18}TAB series. The C_{14}TAB−C_{16}TAB series was carried out at 30 °C, while the C_{16}TAB−C_{18}TAB series was carried out at 40 °C. In the following, the surfactant composition is referred to as $C_{n_{c1}}$-X_1−$C_{n_{c2}}$-X_2, where n_{cn} indicates the number of carbon atoms in the respective surfactant chain, and X_n indicates the mole percent of the respective surfactant of the total surfactant concentration, if not otherwise mentioned.

The heat produced by the hydrolysis−condensation reactions that occur during the synthesis was determined by microcalorimetry. An isothermal Tian-Calvet type microcalorimeter described elsewhere[26] was used. The TEOS was injected in one step inside the microcalorimetric cell in which the surfactant/NH_3/H_2O mixture was stirred by a magnet driven propeller.

Electron Density Reconstruction. The changes in the relative intensity of the reflections suggest that there are changes in the electron density distribution in the mesophase during the course of the reaction. One means of deriving electron density distributions from a limited number of powder diffraction reflections, namely the direct Fourier transformation of the intensity amplitudes, has been described, e.g., by Harper et al.[27] We have used this method for calculating the electron density reconstructions (2D electron density maps) of the 2D hexagonal C_nTAB-silica phase in a similar way as for SBA-15.[28] For the 2D hexagonal phase, the electron density $\rho_e(\mathbf{r})$ can be expressed by a Fourier series of cosines by:

$$\rho_e(\mathbf{r}) = \rho_{\text{average}} + \sum_q A_{\mathbf{q}} \cos(\mathbf{q}\cdot\mathbf{r})$$

in which $A_{\mathbf{q}}$ is the Fourier coefficient, $\mathbf{q}$ is the Fourier vector of the hexagonal lattice, and ρ_{av} is the average electron density. From the X-ray diffraction pattern the integrated intensities were determined by integrating the area under the diffraction peaks, with an individual baseline for each reflection. The absolute values of the Fourier amplitudes $|A_{\mathbf{q}}|$ for the electron can be determined from the integrated intensities by:

$$|A_q| = \sqrt{\frac{I(|q|)|q|^2}{CM(h,k)}}$$

with

$$|q| = 2\pi s = \frac{4\pi}{\sqrt{3}a}\sqrt{h^2 + k^2 + hk}$$

where C is an arbitrary scaling constant giving the difference from the diffraction intensity in theory (in absolute units) to the realative intensity (counts) in an experiment, $M(h,k)$ is the multiplicity of the respective reflections, s is the absolute value of the reciprocal vector, and a is the unit cell parameter. The factor $|\mathbf{q}|^2$ stands for the lorentz correction for the used diffraction geometry (for a more detailed discussion see ref 29). For the 2D hexagonal phase, the multiplicity $M(h,k)$ for the observed reflections (1,0), (1,1), (2,0) is 6, whereas for the (2,1) reflection its value is 12.

The correct phaseing for the Fourier amplitudes $A_{\mathbf{q}}$, i.e., the correct sign + or − for the 4 different Fourier amplitudes, must be solved as the remaining step. Several approaches are reported in the literature to solve the so-called phase problem. We have selected the permutational approach. All possible permutations (16 electron density maps) have been calculated and have been compared with the following model: (i) low electron density in the core regime and (ii) high and smooth electron density in the surrounding silica zone.

Taking into account the boundary conditions and if the origin is set to the center of the cross-section of the cylinder, it is evident that the sign of the first term (1,0) is negative, since the electron density in the silica portion is definitely higher than the electron density in the hydrophobic micellar core. This condition reduces the possible iterations to 8 permutations. Taking into account model assumptions i−ii, the only meaningful phasing from all permutations is − + + −. Further support for the correctness of the phase assignment is given by the fact that this phasing gives a physically reasonable description of the electron density variations for all reaction times. This is mandatory, since the intensity of any of the reflections does not temporarily vanish during the time-window studied, which is a prerequisite for a phase change to occur.

The full width at half-maximum of the reflections was determined by fitting a Lorentzian function to the reflections with individual background subtraction. The instrumental contribution to the broadening of the reflections was assumed to be 4 channels in all cases.

Results and Discussion

The time-resolved in situ synchrotron XRD patterns measured for two mixed surfactant templated silica, C14-50-C16-50 and C16-50-C18-50, are shown in Figure 1, expressed on the linear s-scale (already defined). These diffractograms were chosen as examples, since they highlight the main experimental results. Similar diffractograms were obtained for all the other surfactant compositions studied. The general features of the diffractograms are similar to those previously reported,[13,16] obtained for C16-100 under otherwise similar experimental conditions. At short reaction times, micellar scattering was observed, which decreased in intensity after the hexagonal phase starts to form, around 80 s into the reaction. This implies that the micelles were consumed by the developing mesophase. Since our experimental setup was optimized for the Bragg region, we do not attempt to analyze the micellar scattering in detail, due to limited low-angle resolution. The 2D hexagonal phase (space

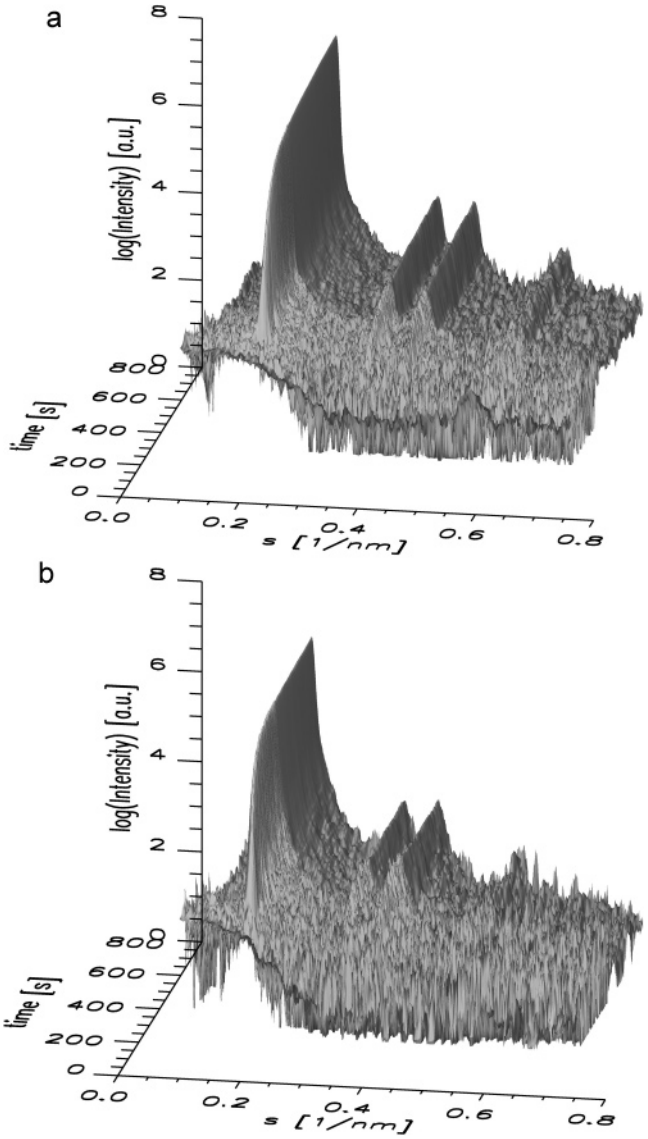

Figure 1. Time-resolved XRD pattern showing the formation of MCM-41 for the (a) C14-50-C16-50 composition measured at 30 °C and (b) C16-50-C18-50 composition measured at 40 °C. See text for details. A data accumulation time of 10 s per frame was used.

group *pmm*6) is formed within 80 s after mixing of the reactants regardless of the synthesis temperature, with well-resolved (10), (11), (20), and (21) reflections. The time at which the first signs of order appear in the diffractogrammes was virtually independent of $n_{c,m}$, but was slightly shorter for the syntheses carried out at 40 °C. Generally, a continuous increase in the intensity of all reflections, a decrease in the repeat distance of the hexagonal phase, and an increase in the intensity ratio between the (11) and (20) reflections with time was observed, which was more pronounced the longer the alkyl chain of the surfactant (see Figure 1). The increase in the intensity ratio between the (11) and (20) reflections occurs mainly within the same reaction time window where the pronounced increase in the intensity of the (10) reflection occurs, within the first 300 s of the reaction. The main obvious difference between the two cases is the lower *d* spacing of the C14-50-C16-50−silicate mesophase (4.31 nm at $t = 600$ s) as compared to that of the C16-50-C18-50−silicate mesophase (4.85 nm at $t = 600$ s). An increase in the *d* spacing with increasing value of $n_{c,m}$ was observed in all cases, as is shown in Figure 2 for corresponding 2D hexagonal silica−CTAB mesophases synthesized with mixed C_{14}TAB−C_{16}TAB

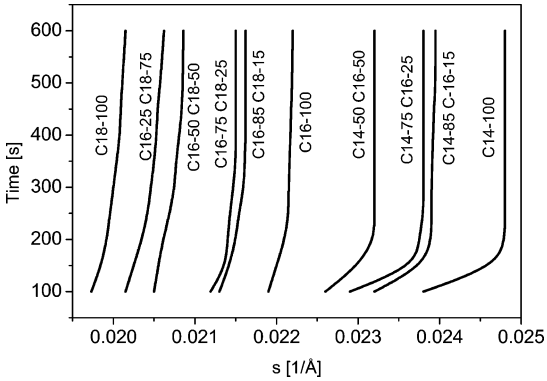

Figure 2. Evolution of the position of the (10) reflection of the 2D hexagonal MCM-41 phase for different mean surfactant chain lengths. The molar concentrations for the respective surfactants given in percentage of the total surfactant concentration are indicated. The C14-100 to C16-100 compositions were measured at 30 °C while the C14-100 to C16-100 compositions were measured at 40 °C.

or C_{16}TAB−C_{18}TAB surfactants as structure directing agents. The decrease in the repeat distance with time was 2−3 Å in all cases, with a kinetics that was virtually completely controlled by the temperature and fairly insensitive to the mean chain length of the structure directing agent under the applied experimental conditions. Note that $s = 1/d$, why different Δs values can correspond to similar Δd values, when the initial *s*-value is different. Note that C_{16}TAB−silica was measured at both temperatures and thus serves as a bridge between the two series. The rate at which the intensity of the (10) reflection increases with time is clearly higher for the measurements carried out at 40 °C, as seen in Figure 1. The effect of the temperature will be discussed in more detail below. However, the formation of the hexagonal silicate−surfactant mesophase from dilute surfactant solutions initially containing mainly spherical micelles must self-evidently involve a transition from a spherical to a rodlike micellar geometry. The tendency to form rodlike micelles increases with increasing surfactant chain length for otherwise similar surfactants, due to the increased hydrophobic attraction between the hydrocarbon chains. The formation of rodlike micelles is further enhanced by the increase in the local surfactant concentration in the phase-separated portion, which is rich in silica and surfactant. An early formation of rodlike micelles may then lead to a slower kinetics of ordering of the 2D hexagonal phase, due to micellar entanglement effects, especially if the rate of condenation is relatively fast, which may explain the decrease in the unit cell contraction kinetics with increasing temperature and increasing mean surfactant chain length. The mean surfactant chain length, $n_{c,m}$, is also determining the size of the unit cell of the hexagonal phase, and the unit cell size increases linearly with $n_{c,m}$, as shown in Figure 3. The increment of the unit cell dimensions ($a = (2/\sqrt{3})d_{10}$) for both the C14−C16 and the C16−C18 series was 2.5 nm/ethyl group, as estimated from the unit cell parameter, *a*, at a reaction time of 600 s. This value is in good agreement with the projection of two times the carbon−carbon bond length of the alkyl surfactant, 2.52 nm.[30] The surfactant concentration is far above the critical micelle concentration, CMC, for all three studied surfactants, which means that the molar fraction of a given surfactant in a micellar aggregate is very close to the corresponding surfactant molar fraction.[7,8] Therefore a linear relationship between the unit cell dimension of the silicate−surfactant mesophase and the mean surfactant chain length of the mixed surfactant assembly can be expected.

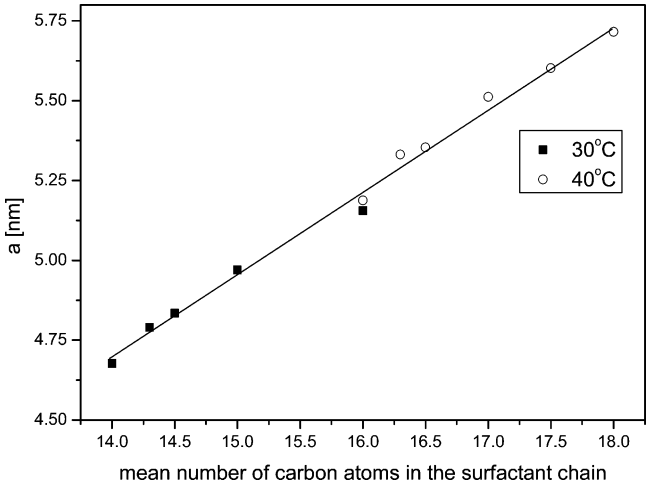

Figure 3. The unit cell dimension, *a*, of the 2D hexagonal phase at a reaction time of 600 s versus the mean surfactant chain length of the surfactant.

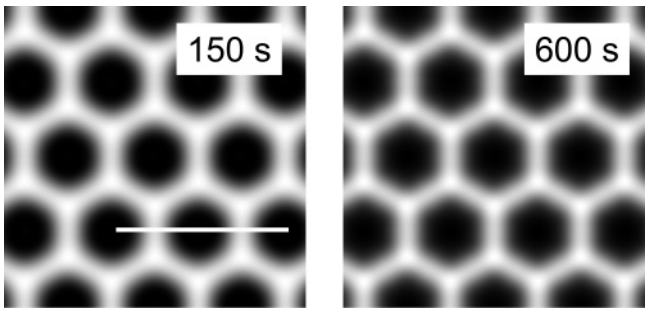

Figure 4. Two-dimensional electron density maps (4 times 4 unit cells) created by using the integrated intensities and positions of the (10), (11), (20), and (21) reflections at specific reaction times as input data: (a) 150 s (*d* spacing 4.065 nm), and (b) 600 s (*d* spacing 4.033 nm) for the C14-100 system. See text for details. White areas correspond to areas of high electron density and dark areas to areas of low electron density.

Electron Density Calculations. The calculated electron density plots for 4 × 4 unit cells are shown in Figure 4 for two reaction times. The electron density within each figure is normalized against their individual max/min electron density. The absolute electron densities cannot be determined in a straightforward way, since we do not know the exact electron density of the silica wall at a given point in time. However, the differences between high and low electron density regions are large enough for qualitative interpretations to be made. Note that the images are not scaled to real space distance. Only selected electron density maps for the C_{14}TAB−TEOS system are shown, as the overall development of all studied compositions was qualitatively the same. Several interesting features are evident from the plots. In Figure 4a, corresponding to the time soon after the formation of the hexagonal mesophase, the electron density maps suggest that the micelles are truly cylindrical. The degree of intermicellar condensation increases gradually with time, as evidenced by the contraction of the mesophase, leading to an overall much more homogeneous electron density distribution in the silica walls, as can be expected (cf. Figure 4a,b). The calculations suggest that the micellar cross-section has a hexagonal shape at longer reaction times. This has previously been observed by TEM for calcined high-quality samples of MCM-41.[31]

The electron density maps suggest that the diameter of the hydrophobic core remains virtually constant during the reaction, which also indicates that the small decrease in the unit cell size occurring during the first minutes after the formation of the hexagonal phase can be attributed to changes in the silica portion of the hybrid material. We again note, however, that this should be taken as a qualitative observation, since the density of the silicate portion is bound to change continuously with time due to ongoing condensation, why an absolute estimation of the wall/core thicknesses becomes very difficult, unless the wall density at any point in time is known. However, the contraction is much smaller for MCM-41 as compared to SBA-15,[28] which is synthesized in the presence of the triblock-*co*-polymer P123 surfactant, and reflects the fact that no silica is present in the palisade layer of the micelles in the MCM-41 synthesis. It has previously been observed that the intensity ratio between the (11) and the (20) reflection increases with time during the formation of MCM-41 type silica,[13,16] titania,[22] and zirconia.[22,23] This effect has been contributed to the increasing degree of condensation in the inorganic portion, leading to an increased Elecron density contrast. It should be noted that the Fourier phasing, $-++-$, obtained in the present work is different from the phasing observed for the 2D hexagonal structure of siliceous SBA-15, which was found to be $--++$.[28] The reason for this difference is the different ratio between the corona thickness and the core radius for the two materials. This is also in agreement with our observation that the intensity ratios of the (11) and (20) reflections increase with decreasing mean surfactant chain length, since the wall thickness to hydrophobic core radius ratio gets closer to that of SBA-15 the shorter the mean surfactant chain length. Therefore caution must be taken before conclusions based on changes in the relative intensities of different reflections as a function of time; the observed increasing I_{110}/I_{200} ratio can only be used as a qualitative measure for the wall density if the correct phasing is known.

Kinetic Reaction Analysis. Né et al.[23] performed a kinetic analysis of the formation of a 2D hexagonal zirconia−C_{16}TAB mesophase taking the ratio between the intensity of the (10) reflection at time *t*, I_t, and the intensity of the same reflection at a point in time (t_{max}) expected to correspond to completion of the reaction, I_{max}, to describe the reaction. The integrated intensity, A_t, rather than the intensity should be used. since time-dependent changes in the full-width-at-half-maximum, fwhm, value may otherwise introduce errors in the analysis. Since all *s*-spacing versus time curves have reached a close to constant value after a reaction time of 600 s, we choose to normalize all integrated intensities against the integrated area of the 10 reflection at this reaction time despite the inherent sources of error, as will be discussed in more detail below. The corresponding plots are shown in Figure 5. All curves have the same shape, with a rapid initial exponential increase followed by a region with a small and virtually linear increase. The shape of the curve is very similar to that of Né et al.[23] As can be seen, all measurements performed at the same temperature nicely fall on top of each other regardless of the value of $n_{c,m}$ There is some inherent scattering in the data, but there is no specific correlation in terms of $n_{c,m}$ and the scattering is attributed to difficulties in assigning a correct value for A_{max}. Also included in Figure 5 are fits to the data based on a first-order reaction Avrami relation

$$\ln(1 - A_{t-t_0}/A_{600}) = k(t - t_0)^n$$

where *k* is the rate constant, and t_0 is the reaction time at which the first sign of the developing mesophase is observed in the diffractogram, and *n* corresponds to the dimensionality of the reaction. Despite some scattering in the data, it is clear that *n*

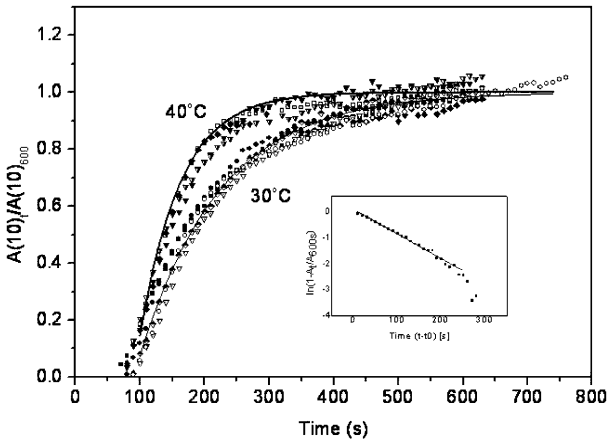

Figure 5. Experimental Avrami plot, where the ratio of the integrated areas of the (10) reflection at time t, A_t, divided by the area A at time $t = 600$ s for all studied mean surfactant chain lengths is plotted against reaction time. The lines are theoretical first-order fits to the data. Inset: the $\ln(1 - A_t/A_{600s})$ vs $(t - t_0)$ plot for C14-50-C16-50.

$= 1$ gives a fairly good descripition of the data in all cases, while other values of n resulted in very poor fits (results not shown). The increased rate of the mesophase formation with increasing temperature together with the insensitivity toward changes in the mean surfactant chain length can be ascribed to an increase in the rate of silicate condensation. Although just having performed measurements at two different temperatures, we still attempt to estimate the enthalpy involved in this first-order reaction according to the Arrhenius formalism, and end up with a value of 42.3 kJ/mol. This is substantially less than corresponding values of about 71 kJ/mol obtained in an earlier study for the formation of siliceous MCM-41,[40] based on FT-IR analysis. However, this difference originates from the fact that we have only so far investigated the initial steps in the formation and not the full reaction, as will be discussed in more detail below.

As shown above, the first-order rate analysis describes this initial step of the mesophase formation fairly well. However, as evidenced by the still slowly increasing intensity of the main reflection the reaction is still proceeding in the sol. We were unfortunately not able to continue the XRD experiments beyond a reaction time of about 900 s due to clogging of the tubing due to an increased agglomeration of the particles. Intuitively this observation suggests that the second reaction step could be connected to further particle growth due to agglomeration paralleled by further aggregate−aggregate condensation. However, there are fundamental inherent problems in applying an Avrami-type analysis to X-ray diffraction data measured on developing mesoscopically ordered inorganic−surfactant hybrid materials. This is due to the fact that the electron density contrast increases continuosly upon increasing silicate condensation accompanied by expulsion of solvent from the mesophase. This also leads to an increase in the measured intensity although the overall quantity of ordered material is not increasing. This leads to an ill-defined end-point of the reaction step under study when the processes of mesophase formation and continuous intermicellar condensation are overlapping, which is the case for most of the normally applied synthesis conditions. This is not accounted for in a simple first-order analysis, like the first-order Avrami formalism, and the rate constants derived by such an analysis will be accompanied by an inherent error that increases with increasing overlapping of these two kinetic events.

Although the Avrami analysis describes our observation fairly well, it is clear that the reaction has not reached completion after 600 s, as evidenced by the continuously increasing value of the integrated intensity of the (10) reflection. Another indication for the reaction still not being completed can be obtained from the analysis of the time-dependency of the fwhm of the reflections. For a homogeneous growth, the fwhm value (and the time-dependency) of the (10) and (20) reflections, here normalized against the position of the (10) reflection, s_{10}, should be the same, while if there is a distribution in the unit cell sizes the fwhm value of the (20) reflection should be larger than that of the (10) reflection. As a representative example, the fwhm plotted versus time for the C14-50-C16-50 case is shown in Figure 6. The fwhm of the (10) reflection decreases fast during the first minute of the reaction and then reaches an almost constant value. A similar time-dependent evolution of the fwhm of the (10) reflection has been observed for mesoscopically ordered aluminosilicates synthesized in the presence of alkylammonium surfactants with use of soluble inorganic precursors, although the kinetics of the mesophase formation was naturally slower.[32] It is evident that the difference in fwhm between the (10) and (20) reflections initially increases quite substantially with reaction time, which is indicative of an increasing second order disorder in the system. However, at reaction times around 600 s, the value of the normalized fwhm value of the (20) reflection, which is more sensitive to disorder than the (10) reflection, starts to decrease again, indicative of a more narrow distribution of repeating distances in the sample at this stage. Here, the measured d spacing also starts to decrease slightly, which also can be attributed to a narrowing of the d spacing distributions in the sample. The initially increasing divergence of the fwhm values with time can only be understood if one assumes that the ongoing silicate condensation leads to a temporary broadening of the unit cell size distribution at intermediate reaction times. This can be related to at least two, partly interlinked, effects. Clearly, the ongoing TEOS hydrolysis and condensation reactions will lead to continuous formation of "new" material also at the stage when the first signs of hexagonal order are observed, as is also reflected by the increasing integrated intensity with time. Furthermore, a dispersion of d spacings can also be present within an area exhibiting hexagonal symmetry, due to local differences in the degree of silicate condensation. Indeed, such an effect has been observed by cryo-TEM for nanosized MCM-41 particles during the initial step of the particle formation.[33] It was observed that the inner part of the particles had a closer packing of the silica-coated micelles compared to the rim of the particle facing the solution. We suggest that both of these effects lead to our observations. The reaction time of about 600 s at which the dispersion in lattice spacings starts to decrease is corresponding to the time after which added hydrophobic swelling agents no longer enter the hydrophobic core of the silicate−surfactant mesophase due to the rigidity of the condensed silica layer under similar synthesis conditions, while addition of the swelling agent at earlier stages of the mesophase formation leads to an increase in the hydrophobic diameter of the hybrid mesophase due to solubilization.[17] This stage of the reaction thus corresponds to the "frozen" state that has been observed by EPR measurements in developing silicate−surfactant systems.[34,37,38] Addition of the swelling agent at intermediate reaction times (135 s) led to the formation of a material with up to three coexisting hexagonal phases, which again can be contributed to the fact that at this stage there are local differences in the degree of condensation but in domains large enough to give rise to Bragg reflections.[17] This is another observation that easily can be understood based on the above discussion concerning the reasons for the time-

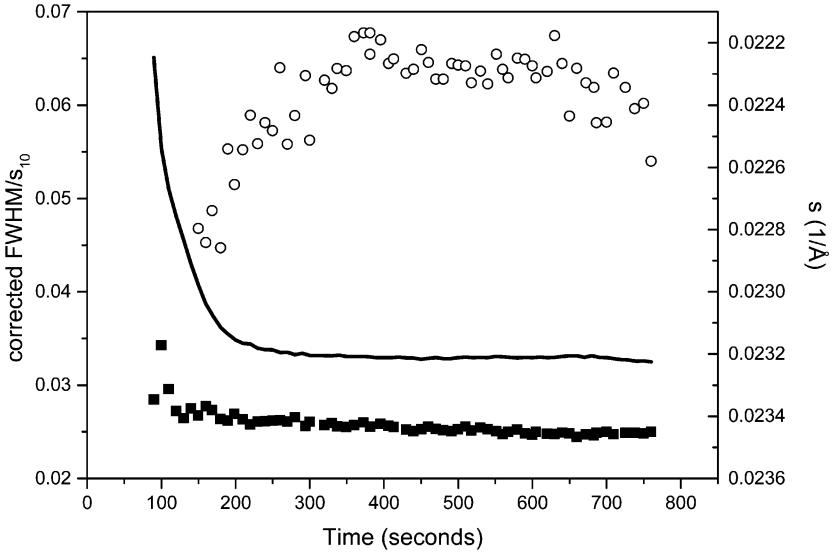

Figure 6. Full-width-at-half-maximum, fwhm, values of the (10) and (20) reflections, normalized against the *s*-value of the 10 reflection, plotted versus time for the C14-50-C16-50 composition. The fwhm values have been corrected for the instrumental contribution assumed to be 4 channels in both cases. Also indicated is the corresponding evolution of the *s*-value with time.

dependent behavior of the fwhm of the (10) and (20) reflections. The same general trends are observed for all studied compositions. However, the normalized fwhm values generally increase with increasing value of $n_{c,m}$, which indicates that the overall degree of initial long-range disorder in the material increases with increasing $n_{c,m}$ within the range of mean surfactant chain lengths studied and under the employed experimental conditions. We tentatively attribute this observation to an earlier formation of rodlike micelles and an increased stiffness of the micelles formed with increasing value of $n_{c,m}$, which leads to a decrease in the long-range order due to micellar entanglement effects. However, it has to be noted that our in situ study only covers the initial stages of material formation, and any subsequent rearrangement effects leading to changes in the long-range order of the materials, for example, due to Ostwald ripening,[35] cannot be addressed on the basis of the present results.

To gain some more information about the kinetics of the reaction steps we carried out a microcalorimetric study to measure the heat effect during the formation of the C16-mesophase. TEOS was added to a solution containing C_{16}TABr in ammonia and water, yielding the same overall concentrations as for the 30 °C synthesis. The resulting heat release curve is shown in Figure 7. It is clear that the reaction consists of 2 main steps that are partly overlapping, in agreement with the fwhm analysis discussed above. As already discussed, the first step is ascribed to the hydrolysis and oligomerization of the silicate species and subsequent mesophase formation and ongoing intermicellar and/or intramicellar condensation. This step is completed within the first 20 min of the reaction, with most of the heat released within the first 5 min of the reaction. This initial step is followed by a much smaller second step, which we ascribe to continuing condensation reactions both between the rodlike silicate−surfactant micelles and between agglomerated particles and to further hydrolysis. This second step reaches completion after a reaction time of about 2 h. Thus the microcalorimetric measurements give clear support for the validity of our approximation for our kinetic analysis of the in situ XRD data. The kinetics of both steps are clearly dependent on the stirring speed during the reaction, which highlights the importance of hydrodynamic forces during the initial emulsification step where the TEOS is hydrolyzed, since the hydrolysis rate must be a function of the exposed surface area of the TEOS

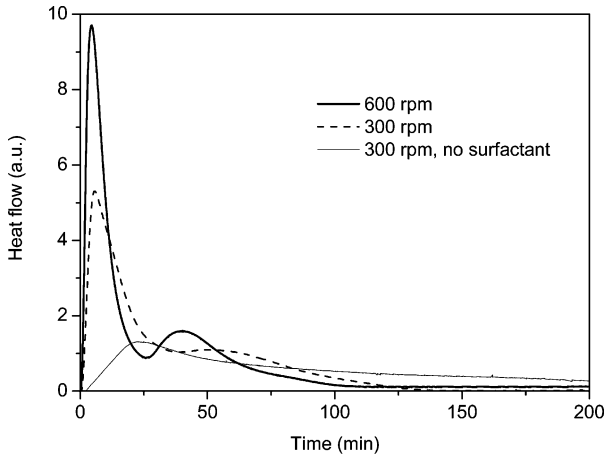

Figure 7. Heat flow versus time measured by microcalorimetry during the synthesis of C16-TEOS MCM-41 at a stirring speed of 600 rpm (thick line) and 300 rpm (dashed line). Also included is the heat flow measured at 300 rpm in the absence of surfactant under otherwise identical conditions (thin line).

droplets.[12,13] However, the calculated heat effect for the formation of the silica surfactant mesophase is about 80 kJ/mol in both cases. The enthalpy connected to the first reaction step is estimated to be 44 kJ/mol and that of the second reaction step to be 36 kJ/mol. The heat released during the hydrolysis and condensation of TEOS in the absence of surfactant is also shown in Figure 7. The overall heat released is very similar as in the case when surfactant is present, but the rate of the reaction is much slower. This result shows that the surfactant indeed has a catalyzing effect on the rate of the reaction as discussed above, but that the energetics involved in the silicate−surfactant interaction is fairly small under the studied conditions.

Mechanistic Implications. Recently, there has been much development in the understanding of the mechanism of formation of mesoscopically ordered, hybrid surfactant−inorganic materials due to an increasing number of in situ studies. Our results can be explained by considering a series of partly overlapping chemical events leading to the formation of the 2D hexagonal phase: (a) hydrolysis of the silicon−alkoxide, (b) formation of silicate oligomers in solution, (c) clustering of poorly condensed silica−surfactant hybrid micelles into flocs,

(d) elongation of the surfactant micelles and parallel formation of domains exhibiting hexagonal order most probably coupled with an increase in the degree of intramicellar silicate condensation, (e) increased intermicellar condensation, and (f) particle growth by agglomeration. This interpretation is well in line with the outcome of recent studies.[5,11,13,23,32−37]

The continuous decrease in the *d* spacing of the hexagonal mesophase after its formation can be directly ascribed to the increase in the density of the silica walls due to increasing intra- and intermicellar condensation reactions. For the silica wall, this naturally leads to a decreased thickness, due to the densification of the silica network. Increasing the temperature from 30 to 40 °C does not lead to any dramatic change in the initiation time, but the growth rate increases by a factor of 1.6 at a constant silicate concentration, while the mean surfactant chain length has little or no influence on the rate of nucleation and growth of the hexagonal phase, within the range of surfactant chain lengths studied. Furthermore, the virtual independency of the kinetics of mesophase formation on the surfactant chain length is contradictory to previous studies[8] where the formation of mesoscopically ordered aluminosilicates was studied under alkaline conditions with alkyltrimethylammonium surfactants with chain lengths varying from 8 to 18 carbon atoms. However, the experimental conditions applied in our study are different with respect to both the pH and the silica source, and the hydrolysis and condensation of TEOS occur fast under our experimental conditions. TEOS-based systems are known to react much faster than corresponding syntheses where soluble inorganic silicates have been used as the precursor for silica.[3,11−15,39,40] Furthermore, the difference in mean surfactant chain length at a given synthesis temperature is limited to two ethyl groups in our case, why the same may not be true for mixed surfactant synthesis with a larger relative difference in surfactant chain length, especially when short-chain surfactants with a high water solubility (high value of the critical micelle concentration) are used.

Acknowledgment. I.B. and M.L. would like to acknowledge the European Community for financial support of this work within the TMR network "MESOP" (ERB-FM-RX-CT-960084) and Elettra (HPRI-CT-1999-00033). P.Å. and M.L. would also like to thank the Finnish National Technology Agency (TEKES) and the Finnish Academy for financial support.

References and Notes

(1) Kresge, C. T.; Leonowicz, M. E.; Roth, W. J.; Vartuli, J. C. *Nature* **1992**, *359*, 710−712.

(2) Beck, J. S.; Vartuli, J. C.; Roth, W. J.; Leonowicz, M. E.; Kresge, C. T.; Schmitt, K. D.; Chu, C. T.-W.; Olson, D. H.; Sheppard, E. W.; McCullen, S. B.; Higgins, J. B.; Schlenker, J. L. *J. Am. Chem. Soc*., **1992**, *114*, 10834−10843.

(3) Monnier, A.; Schüth, F.; Huo, Q.; Kumar, D.; Margolese, D.; Maxwell, R. S.; Stucky, G. D.; Krishnamurty, M.; Petroff, P.; Firouzi, A.; Janicke, M.; Chmelka, B. F. *Science* **1993**, *261*, 1299−1303.

(4) Firouzi, A.; Kumar, D.; Bull, L. M.; Besier, T.; Sieger, P.; Huo, Q.; Walker, S. A.; Zasadzinski, J. A.; Glinka, C.; Nicol, J.; Margolese, D.; Stucky, G. D.; Chmelka, B. F. *Science* **1995**, *267*, 1138−1143.

(5) Zana, R.; Frasch, J.; Soulard, M.; Lebeau, B.; Patarin, J. *Langmuir* **1999**, *15*, 2603−2606.

(6) Khushalani, D.; Kuperman, A.; Coombs, N.; Ozin, G. A. *Chem. Mater*. **1996**, *8*, 2188−2193.

(7) Namba, S.; Mochizuki, A.; Kito, M. *Chem. Lett*. **1998**, *7*, 569−570.

(8) Cheng, Y.-R.; Lin, H.-P.; Mou, C.-Y. *Phys. Chem. Chem. Phys.* **1999**, *1*, 5051−5058.

(9) Patarin, J.; Lebeau, B.; Zana, R. *Curr. Opin. Colloid Interface Sci*. **2002**, *7*, 107−115.

(10) Edler, K. J. *Aust. J. Chem*. **2005**, *58*, 627−642.

(11) Regev, O. *Langmuir* **1996**, *12*, 4940−4944.

(12) Lindén, M.; Schunk, S. A.; Schüth, F. *Angew. Chem., Int. Ed.* **1998**, *37*, 821−823.

(13) Ågren, P.; Lindén, M.; Rosenholm, J. B.; Schwarzenbacher, R.; Kriechbaum, M.; Amenitsch, H.; Laggner, P.; Blanchard, J.; Schüth, F. *J. Phys. Chem B* **1999**, *103*, 5943−5948.

(14) O'Brien, S.; Francis, R. J.; Fogg, A.; O'Hare, D.; Okazaki, N.; Kuroda, K. *Chem. Mater*. **1999**, *11*, 1822.

(15) Rathousky, J.; Schulz-Ekloff, G.; Had, J.; Zukal, A. *Phys. Chem. Chem. Phys*. **1999**, *1*, 3053−3057.

(16) Ågren, P.; Lindén, M.; Rosenholm, J. B.; Blanchard, J.; Schüth, F.; Amenitsch, H. *Langmuir* **2000**, *16*, 8809−8813.

(17) Lindén, M.; Ågren, P.; Karlsson, S.; Bussian, P.; Amentisch, H. *Langmuir* **2000**, *16*, 5831−5836.

(18) Pevzner, S.; Regev, O. *Microporous Mesoporous Mater*. **2000**, *38*, 413−421.

(19) Gross, A. F.; Ruiz, E. J.; Tolbert, S. H. *J. Phys. Chem. B* **2000**, *104*, 5448−5461.

(20) Lind, A.; Andersson, J.; Karlsson, S.; Ågren, P.; Bussian, P.; Amenitsch, H.; Lindén, M. *Langmuir* **2002**, *18*, 1380−1385.

(21) Tiemann, M.; Goletto, V.; Blum, R.; Babonneau, F.; Amenitsch, H.; Linden, M. *Langmuir* **2002**, *18*, 10053−10057.

(22) Lindén, M.; Blanchard, J.; Schacht, S.; Schunk, S. A.; Schüth, F. *Chem. Mater*. **1999**, *11*, 3002−3008.

(23) Né, F.; Testard, F.; Zemb, Th.; Grillo, I. *Langmuir* **2003**, *19*, 8503−8510.

(24) Tiemann, M.; Fröba, M.; Rapp, G.; Funari, S. S. *Chem. Mater*. **2000**, *12*, 1342−1348.

(25) Amenitsch, H.; Rappolt, M.; Kriechbaum, M.; Mio, H.; Laggner, P.; Bernstorff, S. *J. Synchrotron Radiat*. **1998**, *5*, 506−508.

(26) Denoyel, R.; Giordano, F.; Rouquerol, J. *Colloids Surf*. **1993**, *76*, 141−148.

(27) Harper, P. E.; Mannock, D. A.; Lewis, R. N. A. H.; McElhaney, R. N.; Gruner, S. M. *Biophys. J*. **2001**, *81*, 2693-2706.

(28) Flodström, K.; Teixeira, C. V.; Alfredsson, V.; Amenitsch, H.; Lindén, M. *Langmuir* **2004**, *20*, 4885−4891.

(29) Warren, B. E. *X-ray Diffraction*; Addison-Wesley Publishing Company: Reading, PA, 1969; reprinted in 1990.

(30) Evans, D. F.; Wennerström, H. *The Colloidal Domain*, 2nd ed.; Wiley-VCH: New York, 1999.

(31) Alfredsson, V.; Keung, M.; Monnier, A.; Stucky, G. D.; Unger, K. K.; Schüth, F. *J. Chem. Soc., Chem. Commun*. **1994**, 921−922.

(32) Galarneau, A.; Di Renzo, F.; Fajula, F.; Mollo, L.; Fubini, B.; Ottaviani, M. F. *J. Colloid Interface Sci*. **1998**, *201*, 105−117.

(33) Sadasivan, S.; Fowler, C. E.; Khushalani, D.; Mann, S. *Angew. Chem., Int. Ed*. **2002**, *41*, 2151−2153.

(34) Zhang, J.; Luz, Z.; Goldfarb, D. *J. Phys. Chem. B* **1997**, *101*, 7087−7094.

(35) Chan, H. B. S.; Budd, P. M.; Naylor, T. deV. *J. Mater. Chem*. **2001**, *11*, 951−957.

(36) Khodakov, A. Y.; Zholobenko, V. L.; Imperor-Clerc, M.; Durand, D. *J. Phys. Chem. B* **2005**, *109*, 22780−22790.

(37) Ruthstein, S.; Schmidt, J.; Kesselman, E.; Talmon, Y.; Goldfarb, D. *J. Am. Chem. Soc*. **2006**, *128*, 3366−3374.

(38) Ottaviani, M. F.; Galarneau, A.; Desplantier-Giscard, D.; Di Renzo, F.; Fajula, F. *Microporous Mesoporous Mater*. **2001**, *44*−*45*, 1−8.

(39) Ortlam, A.; Rathousky, J.; Schulz-Ekloff, G.; Zukal, A. *Microporous Mesoporous Mater*. **1996**, *6*, 171−180.

(40) Holmes, S. M.; Zholobenko, V. L.; Thursfield, A.; Plaisted, R. J.; Cundy, C. S.; Dwyer, J. *J. Chem. Soc., Faraday Trans*. **1998**, *94*, 2025−2032.